Green Chemistry

PAPER

Biomass-derived Binderless Fibrous Carbon Electrodes for Ultrafast Energy Storage

Received 00th January 20xx,
Accepted 00th January 20xx

DOI: 10.1039/x0xx00000x

www.rsc.org/

R. Berenguer,[a] F. J. García-Mateos,[a] R. Ruiz-Rosas,[b] D. Cazorla-Amorós,[b] E. Morallón,*[c] J. Rodríguez-Mirasol*[a] and T. Cordero[a]

The possibility to store energy efficiently and sustainably at little cost is crucial to prevent climate change and exhaustion of natural resources. In this communication we demonstrate that interconnected and porous carbon fibers easily obtained from lignin exhibit ultrafast charge-discharge and excellent energy density and cyclability performance, to be used as binderless and flexible electrodes in supercapacitors.

Electrochemical capacitors, usually referred to as supercapacitors, are electrochemical devices for electrical energy storage and harvesting applications that can complement or replace batteries when high power delivery or uptake and/or long cycling stability are required. Additionally, these devices improve efficiencies in supply systems (such as internal combustion engines, renewable energy systems, batteries and fuel cells) by storing energy when in excess or not needed. Thus, they are considered as one of the most powerful technologies that will provide a more efficient and sustainable utilization of energy on a short-term and real scenario of increasing energy costs and threatening climate change.[1]

In spite of such relevance, the widespread utilization of supercapacitors has not been achieved due to a high cost to performance ratio. Among different electrode candidates, the last decade has witnessed a very intense research in the capacitance and storage performance of different nanostructured carbons, like graphene, CNTs, fullerenes, CNFs, onions, templated carbons, etc.[1] Nevertheless, apart from the significant progress on fundamental aspects, the complex and expensive manufacture as well as the complicated handling and electrode processing of these carbon materials make uncertain their feasible application. Accordingly, while novel electrode materials and chemistries are being developed to improve the storage performance, further research on simpler and cheaper manufacture and processing is demanded.

Activated carbons (AC) derived from biomass and polymers have been identified as the currently most viable materials for supercapacitors, from both economic and sustainability points of view.[1a] To attain the specifications for widespread commercialization, various issues need to be solved, being the most important to produce AC with a high accessible surface area and a sufficiently high electrical conductivity. On the one hand, biomass and natural polymers show a heterogeneous structure and contain impurities that complicate their processing to produce adequate conductive carbon electrodes. On the other hand, the derived ACs are conventionally obtained as powder or granular materials. Both the particle-like morphology and porosity strongly increase their inter- and intra-particle electrical resistances,[1e] respectively, what makes necessary their processing into electrode pastes (by using auxiliary binders and conductivity promoters). This generates many electric point contacts that decrease their mechanical and chemical stability.[2] Hence the development of binderless porous carbons by a direct route would improve the conductivity and stability of carbon electrodes, and at the same time, it would reduce the time, complexity and the environmental and economic impacts of the overall manufacture. In addition, the possibility of using biomass precursors for the preparation of these electrodes could suppose a unique opportunity for their valorization into high added-value products.

In this communication, we report a sustainable and inexpensive approach to process one of the most abundant polymers in nature, lignin,[3] into binderless flexible carbon electrodes with ultrafast response and overall high-performance for energy storage in supercapacitors. The approach involves the preparation of interconnected and porous carbon fibers (CFs), with submicron diameter and high surface area and conductivity. Particularly, we demonstrate that these materials can be simply but uniquely accomplished by electrospinning and subsequent thermal conversion of a proper lignin into CFs, with an easy control of their connectivity and porosity degree.

The preparation of the biomass-derived fibrous carbon electrodes firstly entails the electrospinning of Alcell®-lignin/ethanol solutions, at ambient temperature and pressure, into submicron-diameter lignin fibers.[4] Electrospinning is a simple and powerful technique for fiber production,[5] whereas the chemical and structural properties of lignin make it a unique precursor for the attainment of carbon materials.[6] Furthermore, Alcell lignin can be dissolved in ethanol[7] and it is the only variety of this polymer that, up to now, has been electrospun at room temperature, directly without any modification

[a] Universidad de Málaga, Andalucía Tech, Departamento de Ingeniería Química, 29071 Málaga, Spain. *E-mail: mirasol@uma.es
[b] Departamento de Química Inorgánica and Instituto Universitario de Materiales, Universidad de Alicante. Apartado 99. Alicante, Spain.
[c] Departamento de Química Física and Instituto Universitario de Materiales, Universidad de Alicante. Apartado 99. Alicante, Spain. *E-mail: morallon@ua.es

† Electronic Supplementary Information (ESI) available: Details of materials characterization, the preparation of the cells, and the determination of gravimetric capacitance, and specific energy and power. See DOI: 10.1039/x0xx00000x

treatment and without any added binder polymer.[8] Interestingly, its pulping (organosolv) process uses ethanol as both delignifying agent and solvent, and exhibits higher pulp yields and it is more environmentally friendly than the production of Kraft lignin, the other more-produced lignin today.[3,4a] Since lignin is a worldwide by-product of pulp and paper industries and will be generated, together with ethanol, what in future may result in wood-to-ethanol bio-refineries,[3] the hereby reported preparation procedure, the resulting electrode materials and their use for energy storage are considered a model example of biomass valorisation, green chemistry and sustainability. In fact, the valorization of lignin into new and highly valuable products is essential for the replacement of petroleum-derived counterparts in multiple applications.[3-5]

After electrospinning, the lignin submicrofibers were thermally air-stabilized and carbonized under various conditions to generate carbon submicrofibers with different connectivity and porosity. The connectivity of fibers, i.e. the production of individual (loose) or interconnected CFs, was controlled by using a suitable heating rate during stabilization. At 0.08 ºC min^{-1}, the heating rate is slow enough to stabilize lignin and prevent its softening during subsequent carbonization,[9] rendering loose CFs (sample LCF-L in Fig. 1a,b). By contrast, thermostabilization of lignin fibers at 0.16 ºC min^{-1} resulted in their partial softening and interconnection at contact points between fibers during carbonization (sample LCF-I in Fig. 1c,d).

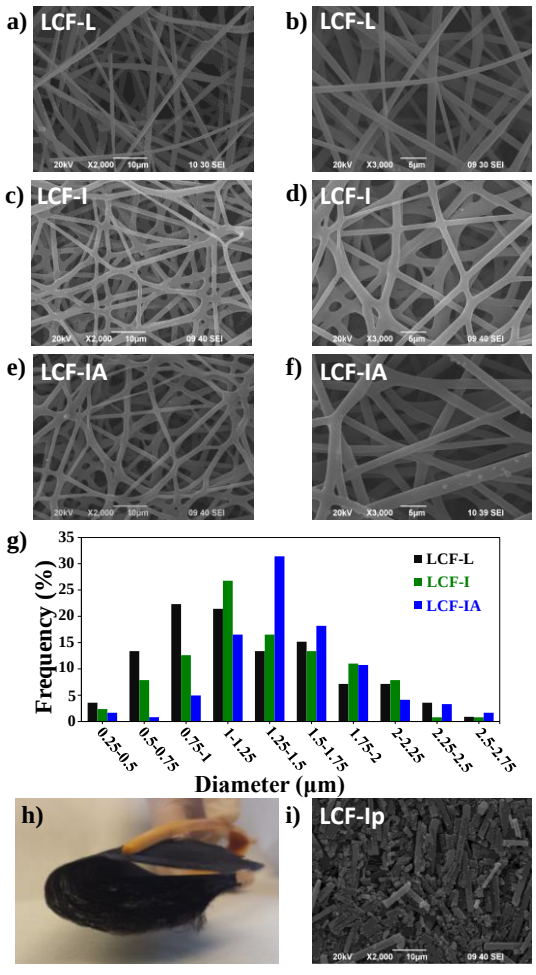

Fig. 1. SEM images, covering different areas, of loose (a,b), interconnected (c,d) and interconnected + partially gasified (e,f) lignin-based CFs; (g) histogram of fiber diameters from SEM images; (h) photograph of a binderless LCF-IA electrode; (i) SEM of a pasted LCF-IA electrode.

Table 1. Specific surface area (S_{BET}); Volume of micropores (Vt); CO and CO_2 evolved from TPD experiments; mass surface composition; and yields of thermostabilization and carbonization treatments and that of the overall production.

	S_{BET}	Vt	TPD (mmol/g)		XPS (wt%)		Yields (wt%)		
Sample	m^2/g	cm^3/g	CO	CO_2	C(1s)	O(1s)	Stab.	Carb.	Overall
LCF-L	690	0.33	0.6	0.5	95.9	4.1	77.0	39.1	30.1
LCF-I	640	0.27	1.0	0.4	95.8	4.2	73.2	38.0	27.8
LCF-IA	1005	0.44	3.5	0.5	95.4	4.6	74.1	34.5	25.6

Both the loose and interconnected CFs exhibited quite similar diameters, mainly in the range of 400 nm to 1.5 µm (Fig. 1g) and are essentially microporous, as deduced from their characteristic type-I N_2 isotherms (Fig. 2a). From these data, the specific surface area (Table 1) and the pore size distribution (Fig. 2b) were calculated (see experimental section). These materials display a high surface area of ca. 700 $m^2 g^{-1}$ and pores in the range 0.4 - 1.3 nm, prevailing those of 0.6 - 0.8 nm. Such microporosity develops directly during carbonization, without any additional activation process, and seems to be related to the high oxygen content in lignin.[4,10] These pores of less than 2 nm-size have been found optimum for double layer charging, whereas the porous structure of CFs favors the accessibility and diffusion of ions,[11] well-known properties beneficial for energy storage in supercapacitors.[1]

On the other hand, the microporosity of the interconnected CFs was further developed (Fig. 2a), again without additional steps, by partial gasification during carbonization in the presence of 1 v% O_2 (5 % burn-off) (LCF-IA sample). This was possible because of the high oxidation resistance of CFs obtained from lignin,[4] again a unique feature of this precursor. Such a high oxidation resistance was confirmed by thermogravimetric analysis (Fig. 2c), illustrating that these CFs start to react in air at very high temperatures (from 550 ºC). The resulting interconnected CFs (sample LCF-IA in Fig. 1e,f) displayed similar diameters (Fig. 1g), but a higher surface area of 1000 $m^2 g^{-1}$ (Table 1), the presence of some wider micropores (d = 1.2-1.7 nm) (Fig. 2b) and a larger concentration of oxygen surface groups (Table 1). Particularly, these groups mainly consisted in phenol- and quinone-like functionalities, as evidenced by their evolution as CO between 600-900 ºC during TPD experiments[12] or their clear contributions at 286.1 and 289.7 eV, respectively, in XPS spectra (Fig. 2d), which can actively contribute to charge storage by pseudocapacitive reactions.[1,12] Thus, while the high carbonization temperatures applied for the obtainment of sufficiently conducting carbons usually restrains their functionalization (≤ 1.0 mmol CO g^{-1} for LCF-L and LCF-I), the hereby reported O_2-activation allows to obtain not only a higher surface area but also an electro-active surface chemistry (3.5 mmol CO g^{-1} for LCF-IA), directly without any post-treatment. In addition, by interconnection the materials became flexible (Fig. 1h), the prerequisite to achieve stretchable and bendable energy storage devices.[13] This is in agreement with the enhanced mechanical behavior caused by inter-fiber bonding of lignin-based carbon fibers prepared by electrospinning.[14]

The structural features of the obtained lignin-based CFs were also analyzed. These properties have been widely related to their

electron conductivity, but they were found practically independent of the different connectivity and porosity of the studied fibers. For instance, the XRD Raman and TEM characterization of the most porous CFs (LCF-IA) is shown in Figures 2e-i. The X-ray diffractogram and the Raman spectrum reflect some common features characteristic of disordered porous carbons. The observed broad (002) and (10) diffraction peaks (Fig. 2e), centered at around 2θ = 25° and 43°, points out the lower crystallinity of the CFs compared to that of the graphite.[15] By using the Scherrer equation,[15a] the mean size of the ordered (crystalline) domains in the perpendicular (Lc) and parallel (La) directions of graphene layers were estimated to be 18 and 33 Å, respectively. On the other hand, the strong D band (at 1355 cm^{-1}) in the Raman spectrum is indicative of the presence of structural defects, and the weaker ones at 1170 and 1515 cm^{-1}, have been ascribed to oxygen surface groups and interstitial defects, respectively (Fig. 2f).[4,16]

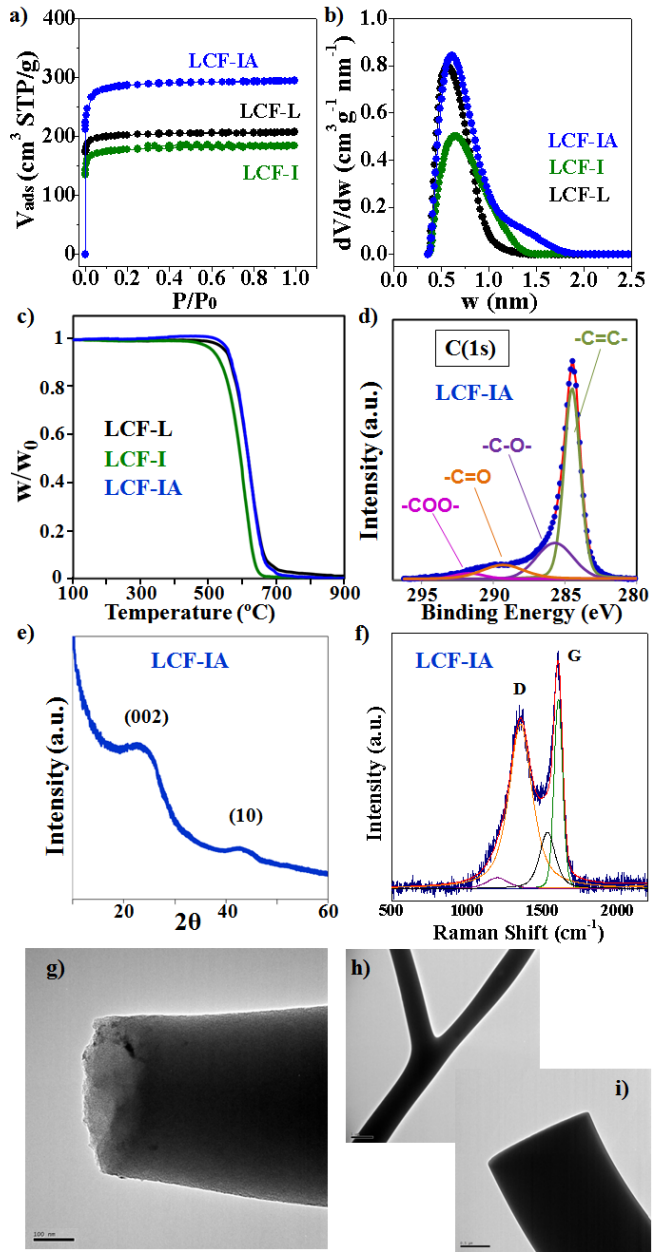

Fig. 2. (a) N_2 adsorption isotherms, (b) pore-size distributions and (c) thermogravimetric analysis of the studied lignin-based CFs. (d) C(1s) XPS deconvoluted spectrum, (e) X-ray diffractogram, (f) deconvoluted first-order Raman spectrum, and (g-i) TEM images (scale bars are 1 µm (g) 0.5 µm (h) and 100 nm (i)) of LCF-IA fibers.

However, TEM reveals that the studied lignin-based CFs exhibit an apparently smooth surface with no macro-/microscopic defects (Fig. 2g), even at the connecting points (Fig. 2h) or ending regions (Fig. 2i). Moreover, although they cannot be compared with those of graphitic or graphitized carbons, the calculated mean crystal dimensions are among the largest of porous carbons prepared at temperatures in the range 700-1000 ºC.[17] These values and the position of the (002) peak (2θ = 25.08 º), with an interlayer spacing of d_{002} = 3.548 Å, being close to that obtained after carbonization of kraft lignin at temperatures as high as 2000 ºC,[16] suggest the existence of an incipient graphitic structure. This can also be deduced from the position of G band in Raman spectrum (1595 cm^{-1}), approaching that of graphite.[15,16a]

It is well known that the thermostabilization step and, therefore, the fabrication of lignin-based CFs is a very slow process.[10] This causes a large energy consumption. In addition, many exhausts evolve during the stabilization and carbonization of lignin precursors.[4b,10] These specifications are inherent to the low glass transition temperature of any lignin source and their high oxygen content. In fact, the slow thermostabilization step is also common of most CF precursors, like PAN, pitches, cellulose, etc.,[9] whereas the evolution of H_2, H_2O, CO, CO_2, light hydrocarbons and waste products (tar and other condensable volatiles) is unavoidable when biomass precursors are used. Although the acceleration of lignin fibers thermostabilization is the aim of intense research, most approaches involve the modification or purification of lignin, the use of thermal pre-treatments or the utilization of polymers and/or chemicals.[18] As a result, additional steps, reagents and energy consumption are involved and by-products could be generated. In this sense, the hereby proposed method for the preparation of interconnected lignin-based CFs reduces the duration of the conventional air thermostabilization process to the half by raising the heating rate, just without any modification of the conventional procedure or any added compound or step. Thanks to be working slightly over the glass transition temperature of the material, interconnection of fibers is also achieved without additives and the activation and functionalization with oxygen surface groups occur simultaneously to thermal processing, without post-treatments. Table 1 collects the yields of thermostabilization and carbonization treatments. Stabilization yields not only account for the condensation and decarboxylation reactions that results in weight losses; they also consider the removal of adsorbed ethanol on the surface of the lignin fibers, which represents around 15% of their initial weight, thus leaving a weight loss accountable to lignin oxidation of only ~10%. The carbonization yields were found to be slightly lower than the direct carbonization of the same alcell lignin upon similar conditions (40.3% wt., not shown for brevity sake). This can be explained considering that the high amount of oxygen groups introduced during the stabilization treatment will be later released as CO and CO_2, thus removing part of the carbon that otherwise would remain in the carbonized product. Nevertheless, the preparation yield is high considering the development of surface area achieved after the carbonization step (which could be seen as a combined carbonization/activation treatment). In fact, for obtaining a similar textural development in the activation of a non-porous carbon fibers from biomass precursors or even from

phenolic resins, a burn-off higher than 20% would be necessary,[19] resulting in a worse use (lower yield when carbonization and activation are both considered) of the raw material. The overall yields (involving stabilization and carbonization treatments) for the production of the reported lignin-based CFS range between 26-30 %, similar to those achieved in biomass based activated carbons[20] and in agreement also with those of CFs obtained from other organosolv-based lignins.[7,21] Hence, not only the described production of lignin fibers by electrospinning of ethanol solutions, but also their thermal processing into interconnected CFs can be considered an environmentally improved route to this type of materials.

The electrochemical behavior of the as-prepared lignin-based CFs was studied in a three-electrode cell in sulfuric acid electrolyte (Fig. 3). Cyclic voltammetry (CV) revealed the ideal rectangular shape of a pure electric double-layer capacitor (EDLC),[1] no matter the connectivity of the CFs (Fig. 3a). In addition, the different CFs displayed a pseudocapacitive contribution at around 0.4 V, related to the electrochemical reaction of quinone-like oxygen functionalities.[12] The significance of this contribution was found proportional to the concentration of these oxygen groups, which can be related to the amount of CO evolved during TPD experiments (Table 1). The formation of such kind of CO-evolving groups is known to occur upon oxygen (ambient conditions) exposure of a carbon surface prepared at high temperatures.[22] From the charge enclosed by the CVs (Fig. 3a), gravimetric capacitance values of 134, 153 and 201 F g^{-1} were obtained for LCF-L, LCF-I and LCF-IA electrodes, respectively. These values seem to be proportional to the combination of their specific surface area and concentration of electroactive CO-evolving groups (Table 1). The stability of the carbon electrodes was studied by step-wise opening of the voltammetric potential window, from the open circuit potential (around 0.3 V) to both negative and positive sides (Fig. 3b). The large cathodic current observed below -0.4 V, corresponding to protons electro-reduction, was probably indicative of the negative stability potential of LCF-L. In the case of LCF-I and LCF-IA this current was shifted towards lower (more negative) potentials. On the positive side, LCF-L also started to show anodic currents at lower overpotentials than LCF-I and LCF-IA. This material was able to reach 1.0 V without apparent voltammetric changes (Fig. 3b). However, after continuous cycling up to this potential a considerable development of pseudocapacitance was observed when compared to a previous CV registered in a narrower potential window (see Fig. 3c). This increase in pseudocapacitance may be attributed to the electrochemical oxidation of carbon surface upon positive polarization in acid media, which produces the generation of electroactive CO-type evolving groups.[23] As a consequence, we concluded that the potential safety limits determined for the three studied materials were at least -0.4 and 0.9 V (vs. Ag/AgCl/Cl-sat.), and that supercapacitor cells constructed using them as binderless electrodes could be operated safely up to 1.3 V. Such a high electrochemical stability is in agreement with the high resistance of the lignin-based CFs to air oxidation (Fig. 2c), and may be related to their characteristic structure and spatial arrangement of the graphitic crystallites and undefective surface (see Fig. 2e-i and the corresponding discussion); as well as the binderless conformation of the electrodes, avoiding the stability problems conventionally derived from the use of additives.

The practical application of the lignin-based CFs as electrodes for supercapacitors was investigated in symmetric two-electrode cells,

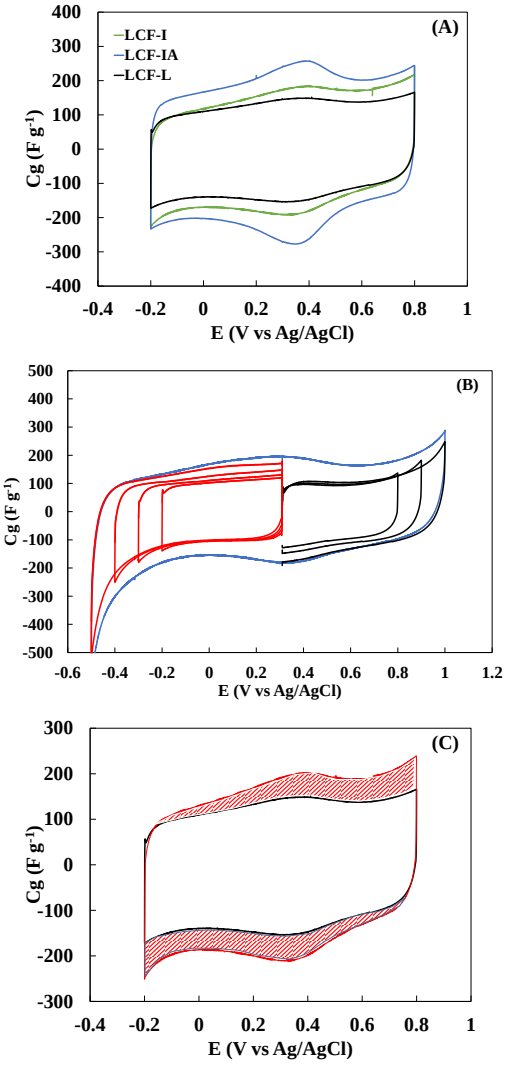

Fig. 3. (a) Steady-state CVs of LCF-L, LCF-I and LCF-IA binderless electrodes; (b) 4th scan CVs of LCF-L electrodes upon step-wise opening of the potential window on the positive and negative sides; (c) CV of LCF-L electrode before and after repetitively cycling up to an expanded potential window of 1.0V. NOTE: All data were obtained in a three-electrode cell; scan rate: 10 mV s^{-1}.

which were constructed by using the as-prepared materials as binderless electrodes, without using any kind of additives or conditioning treatments. The advantages of using interconnected CFs as binderless electrodes can be observed in Fig. 4a, where the response of binderless LCF-I is compared with that of binderless LCF-L and also that obtained for LCF-I processed in the conventional form of an electrode paste (sample LCF-Ip in Fig. 1i), adding Teflon and a carbon black as binder and conductivity promoter, respectively. At low scan rate (100 mV s^{-1}), the three materials render a quite similar electrochemical (CV) response. However, at faster scan rates, for example at 1 V s^{-1}, the carbon paste LCF-Ip shows a sluggish response, while the binderless LCF-I electrode is able to keep the characteristic rectangular-shape CV of EDLCs better than the LCF-L. This difference must be undoubtedly related to differences in fibers connectivity (loose vs interconnected), a feature that is correlated to the conductivity of the electrode.[14] In particular, when the scan rate is raised from 10 to 1000 mV s^{-1} the

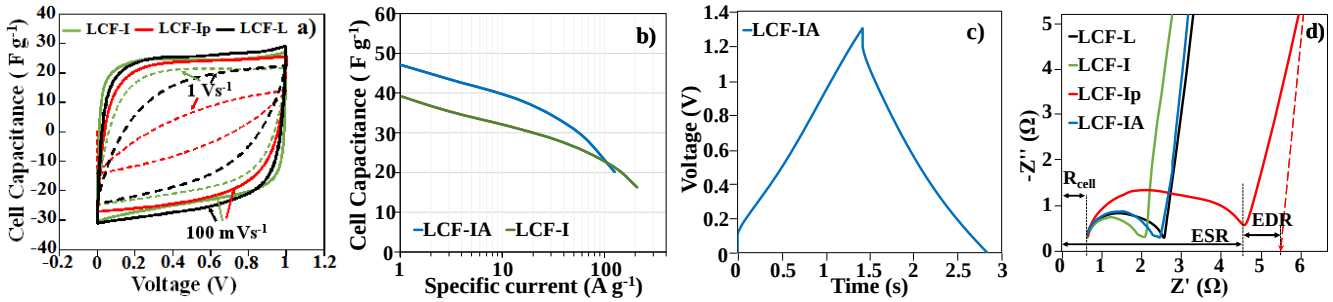

Fig. 4. a) Steady-state CVs from symmetric two-electrode cells of binderless LCF-L and binderless and pasted LCF-I (composition of the carbon paste: 90/5/5 = LCF/Teflon/acetylene black). b) Rate performance for the binderless LCF-I and LCF-IA cells. c) GCD profiles of the binderless LCF-IA cell at 32 A g^{-1} (cut-off voltage: 1.3 V). d) Nyquist plots of freshly constructed two-electrode cells with different electrodes (applied voltage: 50 mV, sine amplitude: 10 mV; frequency ranges: 100 kHz-0.1 Hz).

capacitance retention for the binderless LCF-I electrode (62 %) is higher than that of LCF-L (36 %) and three times higher than for the pasted one (17 % for LCF-Ip), highlighting the beneficial utilization of LCF-I directly as binderless electrodes.

Capacitance retention for the LCF-I supercapacitor cell is higher than those found for seamless carbon forms like activated carbon monoliths.[24] Only advanced porous carbon materials, such as hierarchical porous carbons[25] or electrospun PAN-based CO_2-activated carbon binderless electrodes[26] can match the outstanding performance of LCF-I binderless electrode, though they required the use of more expensive and less environmental carbon precursors or their preparation is burdened by complicated and energy-demanding procedures.

Under galvanostatic charge-discharge (GCD) conditions, the different electrodes display the triangular-shape response characteristic of the charge and discharge processes in EDLCs (Fig. S1). Table 2 compiles a collection of properties for the analysed supercapacitor cells. First, their cell capacitance was found practically independent of the cut-off voltage, slightly increasing up to a maximum value of 1.3 V (Fig. S1 and Table 2). As expected, cell capacitances values at low specific currents are similar between the LCF-L and LCF-I electrodes, being 35 % higher when carbonized in the presence of oxygen (LCF-IA). After a 64-fold increase of the specific current, the capacitance severely dropped for the unconnected electrode (LCF-L). Surprisingly, the interconnected binderless electrode obtained after smooth air activation showed a boosted capacitance while preserving a low ohmic drop (LCF-IA, Fig S1 and Table 2). It can be seen that, although all the electrodes exhibited very low IR drops at 1 A g^{-1}, differences between the cells arises as the applied current increases, with LCF-I and LCF-IA (ohmic drops of 0.186 and 0.207 V) outperforming the results from the LCF-L (0.282 V). The cell resistances were calculated from these values, going down from 3.19 to 2.12 ohms after the interconnection of the carbon fibers. As observed in the table, most of the stored charge was effectively recovered during discharge of the cells, with coulombic efficiencies ranging between 99.0 and 99.5 % in the case of the interconnected electrodes, even when the voltage was increased up to 1.3 V. The energy efficiency of the cells, which is usually an underestimated parameter of supercapacitors, was also measured. It reaches values close to 90 % when working at 1.0 V. When the cut-off voltage was further increased up to 1.3 V, the larger contribution of redox reactions to capacitance leaded to a small decrease (around 3-5 %) in the energy efficiency for all the electrodes, being slightly larger for the electrode with the larger amount of surface functionalities (5.6 % for LCF-IA). Upon raising the applied current intensity from 1 to 64 A g^{-1}, the increasing energy losses due to Joule effect made the energy efficiencies to decay. Nevertheless, the interconnection of fibers seemed to lower these energy losses when working at higher specific currents, at least for 1.3 V operating voltage.

Table 2. Cell gravimetric capacitance (C_g), coulombic (C_{eff}) and energy (E_{eff}) efficiencies, and resistance (R_{cell}) of two-electrode cells constructed with the lignin-based CFs.

		1 A g^{-1}			64 A g^{-1}			
Electrode	**Voltage**	**C_g**	**E_{eff}**	**C_{eff}**	**C_g**	**E_{eff}**	**C_{eff}**	**R_{cell}**
	V	**F g^{-1}**	**%**	**%**	**F g^{-1}**	**%**	**%**	**Ω**
LCF-L	1.0	32	89.1	99.3	19	75.4	99.5	3.19
	1.3	34	86.5	98.9	18	69.2	98.0	
LCF-I	1.0	32	90.2	99.3	27	75.9	99.4	2.12
	1.3	34	86.9	98.9	27	71.1	98.3	
LCF-IA	1.0	45	90.6	99.3	35	71.2	99.8	2.36
	1.3	47	84.8	98.9	29	69.8	99.9	

Owing to their better response, the rate performance of LCF-I and LCF-IA cells was then analyzed upon a wide range of specific currents (Fig. 4b). Considering the maximum cell capacitances and the overall high-enough coulombic and energy efficiencies obtained when working at 1.3 V (Table 2), this was selected as the operational voltage for both cells. Because of their higher surface area and content of electroactive oxygen groups, the interconnected and more activated CFs (LCF-IA) exhibited the highest capacitance, while those without additional activation (LCF-I) showed the best rate performance. For LCF-IA, a cell capacitance of 48.0 F g^{-1} is achieved at the lowest tested specific current. Interestingly, the cell retains 42% of the capacitance when the applied current was raised from 0.25 to an ultrahigh specific current density of 128 A g^{-1}. A comparable storage rate performance, with a lower capacitance but a better capacitance retention (58%), has been also found for the LCF-I. In particular, under an extremely demanding specific current of 32 A g^{-1}, the cell with LCF-IA can be charged and discharged in less than 1.5 s while keeping a high capacitance of 34.1 F g^{-1} and showing only 103 mV of ohmic drop (Fig. 4c).

Moreover, these electrodes show other valuable features for their use in symmetric supercapacitors. On the one hand, both the negative and positive electrodes display quite similar capacitances, causing only a slightly uneven operational potential window (values of ΔV^+ and ΔV^- of 0.69 and 0.61 V, Fig. S2). On the other hand, the potential limits of each electrode reached during the charge of the cell were nearly constant, no matter the used specific current (Fig S2). This stability of the potential windows allows to safely operate this cell at 1.3V under a wide range of current loads, a very interesting feature for systems that require or provide variable source of power.

The observed ultrafast response of the lignin-based interconnected CFs and their superior rate performance is supported by electrochemical impedance spectroscopy (EIS) measurements (Fig. 4d). The low and fairly similar R_{cell} values (first intercept on the Z'axis) in Nyquist plots (around 0.64-0.70 Ω at 100 kHz) observed in all cases reflects the high conductivity of the whole cell, including that of the electrode materials,[27] what may be associated to the suitable properties of lignin to produce ordered carbon structures.[16a] However, clear differences in the semicircle diameters (and the Equivalent Series Resistance (ESR)) were found for the different electrode materials, which are indicative of a remarkable influence of their distinct continuity, connectivity and porosity, or amount of functional groups.[27] The huge increase of resistivity observed for the LCF-I electrode when prepared as a paste highlights the benefits of using binderless materials to obtain higher conductivities. In addition, ca. 40 % reduction in resistance is achieved when the topology of the carbon electrode is changed from loose (LCF-L) to a well-interconnected network of CFs (LCF-I). This is attributed to the increased network connectivity in the interconnected CFs, providing a greater number of pathways for charge transport.[14] Furthermore, the results also indicate that an extra activation of the interconnected CFs (LCF-IA) increases their electrical resistance, probably connected to the presence of a larger amount of electron-withdrawing surface oxygen groups and porosity-derived structural defects.[4b] Nevertheless, in spite of their narrow porosity, all the electrodes showed a low Equivalent Distributed Resistance (EDR),[27] reflecting the low electrolyte resistance within the highly accessible pore system of CFs,[28] especially, in those with ultrafine diameter prepared by electrospinning.[29]

The exceptional performance of the lignin-based fibrous carbon materials was finally highlighted in terms of specific energy and power of the supercapacitor cells in a Ragone plot (Fig. 5a). For comparison purposes, the plot collects also the performance results, among the best reported, of other supercapacitor devices constructed with flexible[30] and electrospun-based[29,31] carbon materials. In terms of energy density, the most activated CFs (LCF-IA) outperform the other tested lignin-based materials in a broad range of power densities, with a maximum energy density close to 10 Wh kg^{-1} and near 5 Wh kg^{-1} when discharged for 1 s (power of 18 kW kg^{-1}). Nevertheless, the maximum deliverable power density is observed for the less porous CFs (LCF-I), showing a maximum power of 61 kW kg^{-1} while storing an energy of 2.0 Wh kg^{-1} that would be delivered in less than 0.2 s in those conditions. By contrast, the loose CFs (LCF-L) and, in much more extent, the pasted discontinuous ones (LCF-Ip) show a marked performance decay at high demanding power densities. Hence, the ultrafast responses of LCF-I and LCF-IA electrode materials are uniquely attributed to their excellent conductivity and the interconnection and long-range

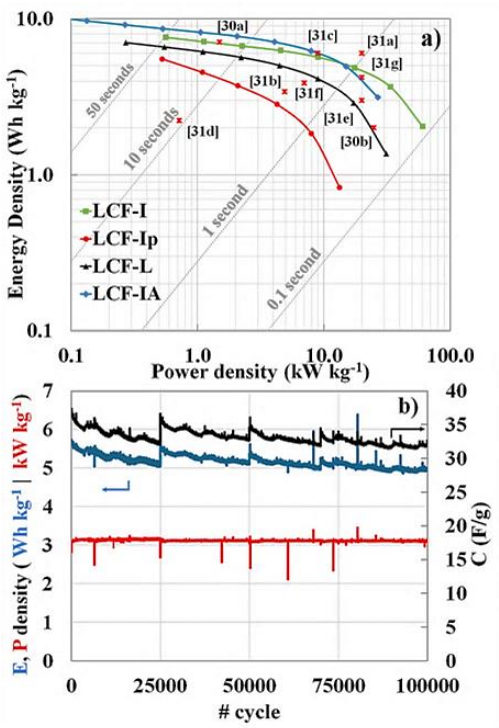

Fig. 5. a) Ragone plots for the studied materials. Literature values from other electrospun-based or flexible supercapacitors are also referred. b) Durability test of the LCF-I cell carried out at 5 A g^{-1}. A resting time of 1 h was imposed each 25000 cycles. (a, b) Operating voltage = 1.3 V.

continuity of the fine electrospun CFs, attained through the control of their stabilization process and by using them as binderless electrodes, respectively. As it is also deduced from the Ragone plot, the energy and power characteristics of the cells made with both kinds of interconnected lignin-based CFs are similar to the best results found for supercapacitors based in electrospun electrodes reported in the literature,[31a,c,g] but without requiring the use of porogens or porosity development treatments. Furthermore, the ultrafast energy delivery exhibited by the reported CFs exceeds by far that of activated carbons and approaches the performance of the top-engineered nanocarbons,[1] just by using an abundant and biorenewable precursor and a simple preparation procedure.

Another important aspect from a practical point of view is the stability of supercapacitors upon charge-discharge cycling. The cycle life of the lignin-based interconnected CFs was evaluated upon 100000 GCD cycles at 5 A g^{-1} and 1.3 V voltage. As it can be observed in Fig. 5b, the cell can practically retain 100 % of its power and around 90 % of total capacitance and energy, with this slight fading being stabilized after the first 50000 cycles. An additional test consisting of a holding voltage ("floating" accelerated test[32]) at 1.3 V during 24 h was conducted after the cycling one. GCD profiles recorded after the cycling and holding test show small changes in the resistivity and the capacitance of the cell (Fig S3a), resulting in a reduced impact in its energy and power (Fig S3b).

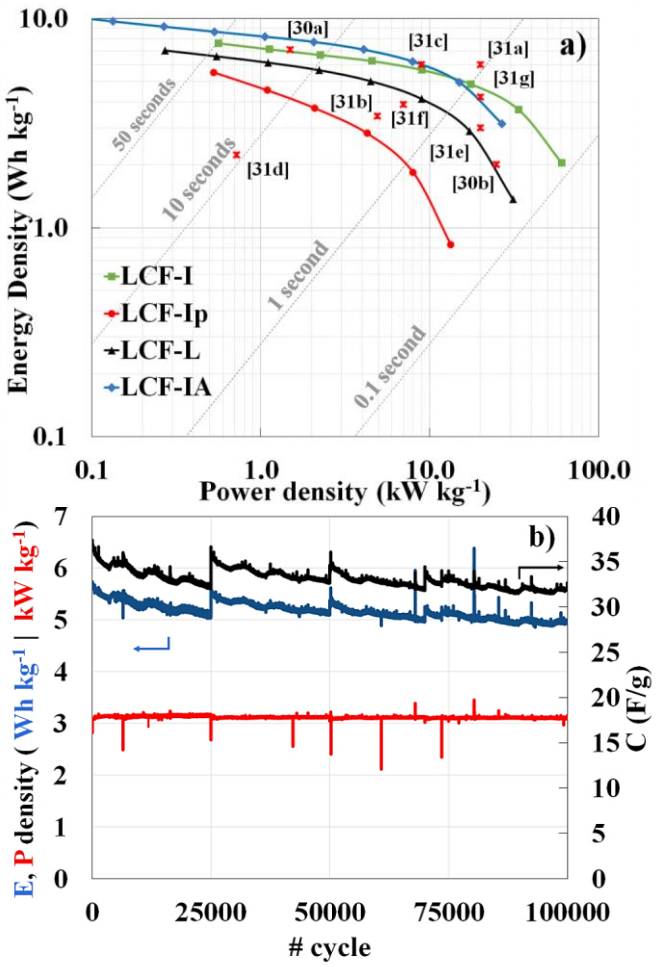

Fig. 5. a) Ragone plots for the studied materials. Literature values from other electrospun-based or flexible supercapacitors are also referred. b) Durability test of the LCF-I cell carried out at 5 A g^{-1}. A resting time of 1 h was imposed each 25000 cycles. (a, b) Operating voltage of 1.3V.

Conclusions

We have demonstrated that an abundant and renewable precursor like lignin can be inexpensively and sustainably processed into interconnected and porous CFs, of submicron diameter, which exhibit an ultrafast storage performance when used as electrode materials for supercapacitor devices. The electrodes are simply prepared by electrospinning of Alcell®-lignin/ethanol solutions and subsequent thermal conversion into CFs, with an easy control of their connectivity and activation degree. Supercapacitor cells can be easily mounted using the CFs as flexible binderless electrodes, showing power and energy densities of up to 61 kW kg^{-1} and 10 Wh kg^{-1}, respectively, which are comparable or superior to the up-to-now top engineered structures, and can retain 100 % and more than 90 % of initial power and energy densities, respectively, after 100000 charge-discharge cycles at 5 A g^{-1}.

Experimental

Preparation of lignin-based CFs

Lignin fibers were prepared by electrospinning of Alcell® lignin-ethanol solutions by using a co-axial configuration.[4] The spinnable solution had a lignin concentration of 45 wt% and a viscosity of 370 cP. The flow rates were 1 mL h^{-1} for the lignin solution (inner spinneret) and 0.1 mL h^{-1} for pure ethanol (outer spinneret). The tip-to-collector distance was 30 cm and the electrical potential difference was 12 kV (the collector was at -6 kV and the tips at +6 kV). The lignin was kindly provided by Repap Technologies Inc. (Canada), while ethanol absolute (p.a. Merck) was used as solvent. The composition of the used lignin was determined by CHNS/O elemental analysis (PerkinElmer® 2400C Instruments) as: 65.9 wt% C; 6.3 wt% H; 0.2 wt% N; 0.00 wt% S; and 27.6 wt% O, while the ash content was 0.00 wt%. Thermostabilization and carbonization treatments were carried out in a horizontal tubular furnace. The thermostabilization was performed under air atmosphere (150 cm^3(STP) min^{-1}) and different heating rates up to 200 ºC, and keeping this final temperature for 36 h. The stabilized materials were carbonized at 10 ºC min^{-1} up to 900 ºC under inert (N_2) or 1 v% O_2 in N_2 atmospheres (150 cm^3(STP) min^{-1}).

Physico-chemical characterization

SEM and TEM images were obtained by a JEOL JSM-6490LV microscope (at 25 kV voltage) and a Philips CM200 microscope (at an accelerating voltage of 200 kV), respectively. The histogram of fiber diameters was constructed from SEM images after the analysis of more than 120 cases for each different CF. The textural properties were characterized by N_2 adsorption-desorption at -196 ºC in a Micromeritics ASAP2020, after outgassed for 8 h at 150 ºC under vacuum. From the N_2 adsorption/desorption isotherms, the apparent surface area (S_{BET}) was calculated by applying the BET equation, and the micropore volume (Vt) by using the t-method. Pore size distribution has been calculated from the N_2 adsorption isotherms considering the proposed 2D-NLDFT Heterogeneous surface model,[33] and by applying the Solution of Adsorption Integral Equation Using Splines (SAIEUS, available online at http://www.nldft.com/) Software. For thermogravimetric analysis (TG), a CI Electronics MK2 balance and samples of 10 mg were used.

The amount of oxygen surface groups was determined as CO and CO_2 desorbed from the samples in temperature-programmed desorption (TPD) analyses. These analyses were carried out up to 940 ºC (10 ºC min^{-1}) in He flow (100 cm^3 STP min^{-1}) in a differential scanning calorimetry–thermogravimetric analysis (DSC–TGA) equipment (TA Instruments, SDT 2960 Simultaneous) coupled to a mass spectrometer (Thermostar, Balzers, GSD 300 T3). The amounts of CO and CO_2 desorbed from the samples were monitored following the 28 and 44 m/z signals, which were previously calibrated by non-isothermal decomposition of calcium oxalate monohydrate (99.999%). XPS data were registered by a 5700C model Physical Electronics apparatus with Mg Kα radiation (1253.6 eV). Raman spectra were recorded with a RENISHAW micro-Raman system using an Ar^+ laser at 514 nm as the excitation source with a spectral resolution of 2 cm^{-1}. The fitting of both the XPS and Raman spectra was done by least squares using Gaussian–Lorentzian peak shapes. The X-ray diffractograms were obtained in a PANalytical

diffractometer (X´Pert PRO) using a CuKα_1 radiation (1.5406 Å). The profile intensities were measured step by step (0.0167° in 2θ) for a whole time of 3000 s. In order to determine the exact angular position of the (002) peak, 10 wt% Si (Aldrich 99.999%) was used as an internal standard. For the application of Scherrer equation, the instrumental broadening contribution was determined by using LaB_6 as crystalline standard.

Electrochemical characterization

The electrochemical measurements have been performed in 1M H_2SO_4 using an Autolab PGSTAT302 potentiostat equipped with FRA module for the Electrochemical Impedance Spectroscopy (EIS), Cyclic voltammetry (CV) and Galvanostatic charge-discharge (GCD) measurements in three electrode cell and an Arbin SCTS Instruments for the galvanostatic charge-discharge experiments and durability tests in two electrode cell. A T-shaped Teflon Swagelock system equipped with gold collectors and Ag/AgCl 3M KCl reference electrode has been used for the assessing the cell performance while registering separately the potential of each electrode. Round-shaped CF pieces were cut in a surface of 0.196 cm^2, the working and counter electrodes being constructed by stacking three round pieces together (total weight between 1.00-1.20 mg) over the gold collectors at each side of the cell, achieving a surface loading in the range of 5-6 mg cm^{-2}. A round piece of Nylon membrane (pore size: 0.45 µm, 7 mm diameter) was used as separator. The electrodes were dried at 80ºC under vacuum for 2 h before determining their weight, and afterwards soaked in the electrolyte for 1 h prior the cell construction and the electrochemical measurements. Further information about the determination of gravimetric capacitances, energy and power density, cell resistance, efficiencies and other relevant parameters are compiled in the supplementary information.

Acknowledgements

Financial support by the Spanish Ministerio de Economía y Competitividad, for the MAT2013-42007-P, P09-FQM-5156R, CTQ2012-36408, JCI2011-10566, JCI-2012-12664 and the joint Spanish-Japanese (PRI-PIBJP-2011-0766) projects, FEDER and the Junta de Andalucía are gratefully acknowledged.

References

1 (a) Y. Zhai, Y. Dou, D. Zhao, P. F. Fulvio, R. T. Mayes and S. Dai, Adv. Mater., 2011, 23, 4828; (b) S. L. Candelaria, Y. Shao, W. Zhou, X. Li, J. Xiao, J. -G. Zhang, Y. Wang, J. Liu, J. Li and G. Cao, Nano Energy, 2012, 1, 195; (c) T. Chen and L. Dai, Mater. Today, 2013, 16, 273; (d) H. Nishihara and T. Kyotani, Adv. Mater., 2012, 24, 4473; (e) M. Inagaki, H. Konno and O. Tanaike. J. Power Sources, 2010, 195, 7880.

2 S. Shiraishi, Boletín del Grupo Español del Carbón, ISSN-e 2172-6094, 2013, 28, 18.

3 A. J. Ragauskas, G. T. Beckham, M. J. Biddy, R. Chandra, F. Chen, M. F. Davis, B. H. Davison, R. A. Dixon, P. Gilna, M. Keller, P. Langan, A. K. Naskar, J. N. Saddler, T. J. Tschaplinski, G. A. Tuskan and C. E. Wyman, Science, 2014, 344, 1246843; (b)

4 (a) M. Lallave, J. Bedia, R. Ruiz-Rosas, J. Rodríguez-Mirasol, T. Cordero, J. C. Otero, M. Márquez, A. Barrero and I. G. Loscertales, Adv. Mater., 2007, 19, 4292; (b) R. Ruiz-Rosas, J. Bedia, M. Lallave, I. G. Loscertales, A. Barrero, J. Rodríguez-Mirasol and T. Cordero, Carbon, 2010, 48, 696.

5 A. Greiner and J. H. Wendorff, Angew. Chem. Int. Ed. 2007, 46, 5670.

6 (a) J. M. Rosas, R. Berenguer, M. J. Valero-Romero, J. Rodríguez-Mirasol and T. Cordero, Front. Mater., 2014, 1:29, 1; (b) W. -J. Liu, H. Jiang and H.-Q. Yu, Green Chem., 2015, doi: 10.1039/C5GC01054C.

7 Y. Ni and Q. Hu, J. Appl. Polym. Sci., 1995, 57, 1441.

8 (a) D. A. Baker and T. G. Rials, J. Appl. Polym. Sci. 2013, 130, 713; (b) E. Frank, L. M. Steudle, D. Ingildeev, J. M. Spörl and M. R. Buchmeiser, Angew. Chem. Int. Ed., 2014, 53, 5262.

9 J. L. Braun, K. M. Holtman and J. F. Kadla, Carbon, 2005, 43, 385.

10 J.-W. Jeon, L. Zhang, J. L. Lutkenhaus, D. D. Laskar, J. P. Lemmon, D. Choi, M. I. Nandasiri, A. Hashmi, J. Xu, R. K. Motkuri, C. A. Fernandez, J. Liu, M. P. Tucker, P. B. McGrail, B. Yang and S. K. Nune, ChemSusChem, 2015, 8, 428.

11 A. Linares-Solano and D. Cazorla-Amorós, Activated Carbon Fibers. In Handbook of Advanced Ceramics, Ed. S. Somiya, Academic Press: Elsevier Inc.; 2013. p. 155.

12 M. J. Bleda-Martínez, J. A. Maciá-Agulló, D. Lozano-Castelló, E. Morallón, D. Cazorla-Amorós and A. Linares-Solano, Carbon, 2005, 43, 2677.

13 K. Xye and B. Wei, Adv. Mater., 2014, 16, 3592.

14 I. Dallmeyer, L. T. Lin, Y. Li, F. Ko and J. F. Kadla, Macromol. Mater. Eng., 2014, 299, 540.

15 (a) M. A. Short and P. L., Jr. Walker, Carbon, 1963, 1, 3; (b) D. D. L. Chung, J. Mater. Sci., 2002, 37, 1475.

16 (a) J. Rodríguez-Mirasol, T. Cordero and J. J. Rodríguez, Carbon, 1996, 34, 43; (b) A. Sadezky, H. Muckenhuber, H. Grothe, R. Niessner and U. Poschl. Carbon, 2005, 43, 1731.

17 (a) M. M. Dubinin, Thermal treatment and microporous structure of carbonaceous adsorbents. Proceedings of the fifth Conference on Carbon. Y. Zhou Ed., Pergamon Press Inc. 1962; (b) Z. Ryu, H. Rong, J. Zheng, M. Wang and B. Zhang, Carbon, 2002, 40, 1131; (c) X. Ma, H. Yang, L. Yu, Y. Chen and Y. Li Materials 2014, 7, 4431.

18 (a) E. Sjöholm, G. Gellerstedt, R. Drougge and I. Brida, WO 2012/112108A1; (b) E. Sjöholm, G. Gellerstedt, R. Drougge and I. Norberg, WO 2013/112100A1; (c) S. Kubo and J. F. Kadla J. Polym. Environ., 2005, 13, 97; (d) S. Hu and Y.-L. Hsieh, J. Mater. Chem. A, 2013, 1, 11279; (e) I. Dallmeyer, L. T. Lin, Y. Li, F. Ko and J. F. Kadla, Macromol. Mater. Eng., 2013, 298, 1; (f) W. Qin and J. F. Kadla, J. Appl. Polym. Sci., 2012, 126, E203; (g) J. Lin, S. Kubo, T. Yamada, K. Koda and Y. Uraki, BioResources, 2010, 7, 5634.

19 (a) A. Oya, S. Yoshida, J. Alcaniz-Monge and A. Linares-Solano, Carbon, 1996, 34, 53; (b) P. T. Williams and A. R. Reed, Biomass Bioenerg., 2006, 30, 144; (c) W. M. Qiao, M. Huda, Y. Song, S.-H. Yoon, Y. Korai, I. Mochida, O. Katou, H. Hayashi and K. Kawamoto, Energy Fuels, 2005, 19, 2576.

20 H. Marsh and F. R. Reinoso, Activated Carbon, Elsevier, 2006.

21 S. Kubo,,Y. Uraki and Y. Sano. Carbon. 1998, 36, 1119.

22 T. J. Bandosz, in Carbon Materials for Catalysis, eds. P. Serp and J. L. Figueiredo, John Wiley & Sons, Inc., 2008, pp. 45–92.

23 (a) R. Berenguer, J. P. Marco-Lozar, C. Quijada, D. Cazorla-Amorós, E. Morallón, Carbon 2009, 47, 1018; (b) R. Berenguer, H. Nishihara, H. Itoi, T. Ishii, E. Morallón, D. Cazorla-Amorós and T. Kyotani, Carbon, 2013, 54, 94; (c) Z. Tabti, R. Berenguer, R. Ruiz-Rosas, C. Quijada, E. Morallón, D. Cazorla-Amorós. Electrochemistry 2013, 81, 833.

24 V. Ruiz, C. Blanco, R. Santamaría, J. M. Ramos-Fernández, M. Martínez-Escandell, A. Sepúlveda-Escribano and F. Rodríguez-Reinoso, Carbon, 2009, 47, 195.

25 D.-W. Wang, F. Li, M. Liu, G. Q. Lu and H.-M. Cheng, Angew. Chem. Int. Ed., 2008, 47, 373.
26 (a) Y. Gao, V. Presser, L. Zhang, J. J. Niu, J. K. McDonough, C. R. Pérez, H. Lin, H. Fong and Y. Gogotsi, J. Power Sources, 2012, 201, 368; (b) C. Kim, J. Power Sources, 2005, 142, 382; (c) E. J. Ra, E. Raymundo-Piñero, Y. H. Lee and F. Béguin, Carbon, 2009, 47, 2984.
27 R. Kötz and M. Carlen, Electrochim. Acta, 2000, 45, 2483.
28 M. J. Bleda-Martínez, D. Lozano-Castelló, D. Cazorla-Amorós and E. Morallón, Energy Fuels, 2010, 24, 3378.
29 M. Inagaki, Y. Yang and F. Kang, Adv. Mater., 2012, 24, 2547.
30 (a) W. Liu, X. Yan, J. Lang, C. Peng and Q. Xue, J. Mater. Chem., 2012, 22, 17245; (b) S. H. Aboutalebi, R. Jalili, D. Esrafilzadeh, M. Salari, Z. Gholamvand, S. Aminorroaya Yamini, K. Konstantinov, R. L. Shepherd, J. Chen, S. E. Moulton, P. C. Innis, A. I. Minett, J. M. Razal and G. G. Wallace, ACS Nano, 2014, 8, 2456.
31 (a) E. J. Ra, E. Raymundo-Piñero, Y. H. Lee and F. Béguin, Carbon, 2009, 47, 2984; (b) A. Kurniawan, L. K. Ong, F. Kurniawan, C. X. Lin, F. E. Soetaredjo, X. S. Zhao and S. Ismadji, RSC Adv., 2014, 4, 34739; (c) C. Ma, Y. Li, J. Shi, Y. Song and L. Liu, Chem. Eng. J., 2014, 249, 216; (d) C. Lai, Z. Zhou, L. Zhang, X. Wang, Q. Zhou, Y. Zhao, Y. Wang, X.-F. Wu, Z. Zhu and H. Fong, J. Power Sources, 2014, 247, 134; (e) T. Le, Y. Yang, Z. Huang and F. Kang, J. Power Sources, 2015, 278, 683; (f) T. Wang, D. Song, H. Zhao, J. Chen, C. Zhao, L. Chen, W. Chen, J. Zhou and E. Xie, J. Power Sources, 2015, 274, 709; (g) C. Tran and V. Kalra, J. Power Sources, 2013, 235, 289.
32 D. Weingarth, A. Foelske-Schmitz and R. Kötz, J. Power Sources, 2013, 225, 84.
33 J. Jagiello and J. P. Olivier, Carbon 2013, 55, 70.